Korhonen, Marko; Wallgren, Kristian; Puisto, Antti; Alava, Mikko; Vuorinen, Ville

Shear localization in large amplitude oscillatory shear (LAOS) flows of particulate suspensions

Published in:
Physical Review Fluids

DOI:
10.1103/PhysRevFluids.6.033302

Published: 15/03/2021

Document Version
Publisher's PDF, also known as Version of record

Please cite the original version:
Korhonen, M., Wallgren, K., Puisto, A., Alava, M., & Vuorinen, V. (2021). Shear localization in large amplitude oscillatory shear (LAOS) flows of particulate suspensions. *Physical Review Fluids*, *6*(3), Article 033302. https://doi.org/10.1103/PhysRevFluids.6.033302

Shear localization in large amplitude oscillatory shear (LAOS) flows of particulate suspensions

Marko Korhonen,* Kristian Wallgren, Antti Puisto, and Mikko Alava
Department of Applied Physics, Aalto University, P.O. Box 11100, FI-00076 AALTO, Finland

Ville Vuorinen
Department of Applied Mechanics, Aalto University, P.O. Box 14100, FI-00076 AALTO, Finland

(Received 21 September 2020; accepted 1 March 2021; published 15 March 2021)

Strong shear localization effects are observed in large amplitude oscillatory shear (LAOS) simulations of a particulate suspension. Here, the structural response of this complex fluid is completely viscous and governed by the general shear-driven diffusion model by Phillips *et al.* [Phys. Fluids **4**, 30 (1992)]. When coupled to oscillatory shear in LAOS, this model is shown to produce concentration gradients, which imply the existence of regions of disparate viscosities across the simulated measurement gap. This suggests the presence of strong shear localization which is conceived even though the intrinsic flow curve of the model is monotonic, and the simulated geometry is a planar Couette setup, expected to display simple shear flow characteristics. This shear localization is generated due to the oscillatory shear at the shearing plate, which, therefore, induces accelerating motion. The subsequent inertial effects act as perturbations in the nonlinear response of the fluid structure to shear and are sufficient to trigger significant localization in the flow. Due to the ubiquitous nature of shear-driven diffusive mechanisms in complex fluids, these results suggest shear localization to be an integral feature of a LAOS measurement of many complex fluids.

DOI: 10.1103/PhysRevFluids.6.033302

I. INTRODUCTION

Accurate and consistent characterization of complex fluids is a vital issue in both academia and industry. Factors hampering the efficient extraction of key rheological quantities include wall slip [1,2], shear bands [3–6], and other nonlinear phenomena occurring at high deformations of the sample [7]. During a measurement, these complications may be perpetual or transient in nature where the latter have proven particularly insidious and difficult to predict accurately. For instance, whereas steady-state shear banding has been associated with a mechanical instability in the intrinsic flow curve of a complex fluid [8,9], transient shear banding has been observed for fluids with simple monotonic flow curves as well [10]. Although there have been theoretical developments addressing this issue [6,11], these studies have not explicitly addressed the issue of flow-concentration coupling. Therefore, the role of inertia in triggering shear localization in a fluid exhibiting such a behavior has not been considered in theoretical studies.

Recently, large amplitude oscillatory shear (LAOS) has reemerged as a possible concept to combat some of these issues arising in experiments. This methodology is endorsed as a means to analyze a more extensive variety of soft materials and accurately probe the response of the complex fluids in the nonlinear regime associated with high deformations [7] and to even provide parameters

*marko.korhonen@aalto.fi

for constitutive modeling [12,13]. Here, we illustrate that the LAOS technique can trigger significant shear localization as reported in Ref. [14] in elementary geometries for even a fluid of a relatively simple structural response, such as the one exhibited by repulsive hard spheres in a suspension. In contrast to the earlier numerical studies reported in the literature [7,15–17], we wish to emphasize that the current model does not: (1) employ any form of elasticity to obtain a shear-localized flow profile and describes a fluid with completely viscous response. Furthermore, (2) the model is based on physically motivated mechanical interactions, and (3) it allows for local variations in concentration and, subsequently, flow-induced phase separation.

Indeed here, the structural response of the fluid is dictated by shear-driven diffusive dynamics of the particles in suspensions [18–22], which we simulate in a planar Couette geometry experiencing oscillatory shear. Despite the relative simplicity and generality of the model and the utilized geometry, we are able to show that large amplitude oscillatory shear induces considerable flow localization effects. These are the result of the inherent accelerating motion of the oscillating boundary condition in LAOS, which induces significant inertial effects equivalent to those in startup flows [23,24]. These then are capable of triggering structural heterogeneities when coupled to the fluid's nonlinear structural response to shear, leading to shear localization due to flow-concentration coupling, which has been reported for soft glasses [25–27] and hard spheres under LAOS [28]. In practice, these heterogeneities may show up as regions of distinct viscosities. We also argue that due to the generality of this model, flow localization should be considered an integral part of the LAOS methodology to avoid erroneous conclusions regarding the constitutive characteristics of the sample. Based on the observations in this paper, significant shear localization effects are predicted as the inverse viscous timescale of the system and the oscillation frequency of the measuring apparatus coincide, provided that the particles are not dominated by Brownian motion, i.e., the mean particle size approaches the granular limit.

II. METHODS

A. Dimensional form of the model

Pursuing simplicity, a well-established model system for a particulate suspension with mechanical (collision) interactions is provided by the work of Leighton and Acrivos [18], which was furthered by Phillips and co-workers [29]. In this framework, the fluid is treated as a hard-sphere suspension, for which multibody collisions and other nonlinear phenomena (elasticity) can be neglected at moderate volume fractions and particles collide solely due to their relative motion driven by shear flow. Accordingly, the continuum limit diffusion model by Phillips *et al.* [29] originally designed and successfully applied to model polymethyl methacrylate suspensions is chosen. This model assumes geometrically isotropic hard spheres susceptible to shear-driven diffusive motion. In the continuum limit, this motion influences the volume fraction of the particles,

$$\frac{\partial \phi(y)}{\partial t} = -\partial_y(N_c + N_\eta + N_b) = -\partial_y N_t, \tag{1}$$

$$N_c = -K_c\, a^2(\phi^2 \partial_y|\dot{\gamma}| + \phi|\dot{\gamma}|\partial_y\phi), \tag{2}$$

$$N_\eta = -K_\eta|\dot{\gamma}|\phi^2 a^2\left(\frac{\partial_\phi \eta}{\eta}\partial_y\phi\right), \tag{3}$$

$$N_b = -D\,\partial_y\phi, \tag{4}$$

where ϕ is the mean volume fraction of the hard spheres K_c, K_η, and D are constants, a is the particle diameter, and $\dot{\gamma} = \partial_y u_x$ whereas $|\dot{\gamma}| = \sqrt{\dot{\gamma}^2}$. N_c describes the particle flux due to variations in the two-body collision frequency of hard spheres across the sheared suspension region. The rationale behind this flux is that particles are prone to migrating from regions of higher collision frequency towards regions of lower collision frequency. The second term N_η denotes the net flux of particles to regions of smaller particle density. Physically, this flux, therefore, describes a situation where

particles attempting to enter these densely occupied areas are more susceptible to being deflected back. Furthermore, N_b is the Brownian motion due to finite temperature, becoming more dominant with decreasing particle diameter a. Here, since we are primarily focused on rather large particle sizes, we choose a very minor value for D so as to have no conceivable effect on the acquired simulation results. However, this small diffusive component in the complete system of equations does provide additional stability to the nonlinear and numerically stiff equations involved. Finally, N_t refers to the total flux due to the various flux terms.

Although the structural response of the fluid to shear is outlined above, the appropriate flow mechanics have to be supplied as well. Here, we consider the (incompressible) Navier-Stokes equations in a planar Couette LAOS flow scenario,

$$\partial_x u_x = 0, \tag{5}$$

$$\partial_t u_x = \partial_y \left(\frac{\eta}{\rho} \partial_y u_x \right), \tag{6}$$

$$\gamma|_{r_a}(t) = \gamma_0 \sin(\omega t) \Rightarrow \dot{\gamma}|_{r_a} = f\gamma_0 \cos(\omega t) = \frac{u_x|_{r_a}}{h} = f\gamma_0 \sin(\omega t) + \delta \approx u_x|_{r_a}$$

$$= hf\gamma_0 \sin(\omega t) \stackrel{\text{def}}{=} v_a \sin(\omega t) = v_a \sin(2\pi f t), \tag{7}$$

$$u_x|_{r_b} = 0, \tag{8}$$

$$N_t \hat{n}|_{r_a} = 0, \tag{9}$$

$$N_t \hat{n}|_{r_b} = 0, \tag{10}$$

where u_x is the fluid velocity (x component), ρ is the density of the fluid, η is the dynamic viscosity of the fluid, and r_a (r_b) refers to the shearing (stationary) plates in a planar Couette geometry. Additionally, h is the gap width in the simulated planar Couette setup, and v_a is the magnitude of the linear velocity at the shearing plate, whereas f presents the frequency of the time-dependent shear in a LAOS protocol. Since the particles cannot penetrate the stationary and shearing plates, the total flux N_t in the normal direction of the plate surfaces (unit vectors $\hat{n}|_{r_a}, \hat{n}|_{r_b}$) has to equal zero. Unlike the original authors in Ref. [29], we have included the time-dependent term $\partial_t u_x$ in the momentum equation above. Although this term may be routinely neglected in rheological modeling of continuous flow, it is of vital importance here: The finite inertial effects experienced by a particulate suspension undergoing such a flow are also accounted for by this term.

Finally, the key issue is to incorporate the structural presentation in Eq. (1) to the flow quantities that are present in the Navier-Stokes equations. In the original paper [29], the authors achieved this conveniently by relating the solid volume fraction to the local viscosity of the suspension via the empirical Krieger-Dougherty function,

$$\eta = \eta_0 \left(1 - \frac{\phi}{\phi_{\max}} \right)^{-k}, \tag{11}$$

where η_0 is the viscosity of the solvent, $\phi_{\max}$ is the jamming limit for the solid phase (for these simulations involving monodisperse particle size distributions, the random close-packing limit 0.68 [30]) and k is a fitting exponent. To simplify the computations, we set $k = 2$, which is also known as the Mason, Pierce, and Quemada model [31]. This agrees both qualitatively and quantitatively with numerous complex fluids and is theoretically justified by examining the self-diffusivity and the number of particle contacts as $\phi_{\max}$ is approached. This viscosity function provides the link between the structural model and the Navier-Stokes equations, which now form a closed system of equations, and are, therefore, expected to provide a uniquely defined solution.

Naturally, the model presented here is a simplification, which has certain limitations: It effectively isolates the large-scale concentration variations from microstructural ordering leading to non-Newtonian local behavior of dense particle suspensions under shear flow at volume fractions above 0.4 [32,33]. This, in turn, may lead to shear thickening and even erratic flow [34,35]. However, since in a LAOS protocol the shear direction is reversed periodically, we expect the microstructural ordering to be insignificant.

B. Nondimensionalization of the system

It should be emphasized that the system of equations presented in the previous section is inherently difficult to solve numerically since it involves both nonlinearity [the terms in Eq. (1)] as well as stiffness due to the contrasting timescales of the (slow) diffusion equation and both the (comparatively rapid) Navier-Stokes equations and the oscillations at the shearing plate. To remedy some of these issues, recasting the system in a dimensionless form is warranted, and the subsequent simulations are performed in this format. This choice also allows for more insight into the underlying dynamics of the system, albeit at the cost of an increased level of abstraction.

Therefore, we proceed by nondimensionalizing the system with the following choices (* denoting the dimensionless quantity):

$$u_x^* = \frac{u_x}{U}, \quad x^* = \frac{x}{L}, \quad \phi^* = \frac{\phi}{\phi_{\max}}, \quad \frac{d}{dr^*}\frac{1}{L} = \frac{d}{dr^*}\frac{dr^*}{dr} = \frac{d}{dr},$$

where U (L) is the characteristic velocity (length scale) in the system. Here, a natural choice for these quantities is the magnitude of the linear velocity at the shearing plate $U = v_a$ and the length of the simulated planar Couette gap $L = h$. These choices then lead to the nondimensionalized form of the Navier-Stokes equations as well as a dimensionless diffusion model,

$$\partial_{x^*} u_x^* = 0, \tag{12}$$

$$\partial_t u_x = \partial_{y^*}\left(\frac{1}{\tau_{\text{visc}}}\partial_{y^*} u_{x^*}\right), \tag{13}$$

$$\partial_t \phi_* = -\partial_{y^*}(N_c^* + N_\eta^* + N_b^*) = -\partial_{y^*} N_t^*, \tag{14}$$

$$N_c^* = -K_c \frac{U a^2}{L^3}\phi_{\max}([\phi^*]^2 \partial_{y^*}|\dot{\gamma}^*| + \phi^*|\dot{\gamma}^*|\partial_{y^*}\phi^*), \tag{15}$$

$$N_\eta^* = -K_\eta\, |\dot{\gamma}^*|[\phi^*]^2 \frac{U a^2}{L^3}\phi_{\max}\left(\frac{\partial_{\phi^*}\eta}{\eta}\partial_{y^*}\phi^*\right), \tag{16}$$

$$N_b^* = -\frac{D}{L^2}\partial_{y^*}\phi^*, \tag{17}$$

$$\frac{1}{\tau_{\text{visc}}} = \frac{\eta}{\rho L^2} = \frac{\eta_0}{\rho L^2}(1-\phi^*)^{-k}, \tag{18}$$

$$u_x^*|_{r_a^*} = \sin(2\pi f t), \tag{19}$$

$$u_x^*|_{r_b^*} = 0, \tag{20}$$

$$N_t^* \hat{n}|_{r_a^*} = 0, \tag{21}$$

$$N_t^* \hat{n}|_{r_b^*} = 0, \tag{22}$$

where τ_{visc} is the local viscous timescale.

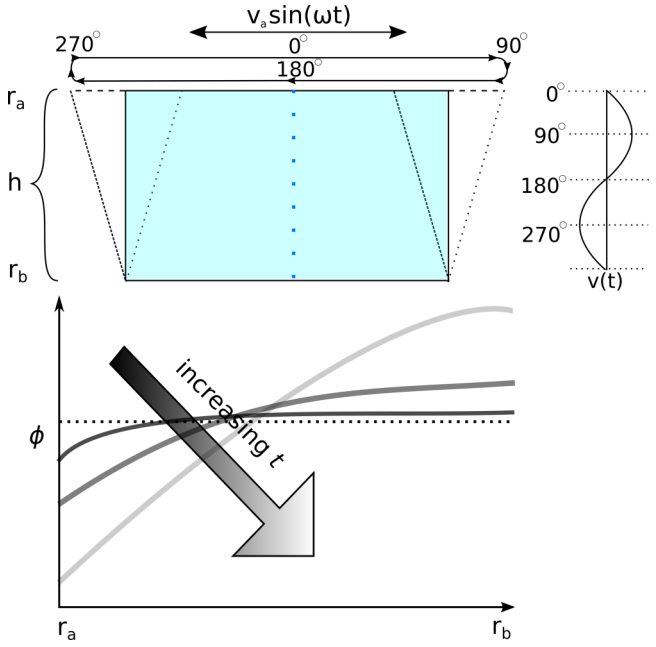

FIG. 1. The parallel plates geometry utilized in the LAOS simulations. The fluid is confined between two plates. Here, one plate remains stationary whereas the other plate sustains a sinusoidal velocity profile with respect to time t with an amplitude v_a and angular frequency ω. An ideal fluid experiences this sinusoidal boundary velocity along the moving plate as plotted on the right-hand side of the figure. In the lower figure, the expected concentration (volume fraction) profile across the gap is depicted in the event of shear localization. Due to diffusive nature of the model, the shear localization is accompanied by spatial variations in the volume fraction with no clearly defined interface.

We are left with reviewing the problem geometry, a planar Couette setup in which these equations are implemented as well as the numerical discretization procedures. The former is depicted in Fig. 1 where the fluid is confined between two parallel plates with a distance h apart from each other. Despite no gravity, we refer to the plates as upper (r_a) and lower (r_b) as visualized in Fig. 1. The lower plate remains stationary, whereas the upper plate follows a temporally sinusoidal velocity profile. The fluid is, therefore, subject to an oscillatory shear and experiences an accelerating flow at the boundary with the upper plate due to the finite density. These finite inertial effects will significantly alter the expected flow behavior of even structurally uncomplicated complex fluids, such as the one described via Eqs. (5), (6), (1), and (11). This is in stark contrast to the routinely assumed Stokes flow conditions where the inertial terms are neglected in the Navier-Stokes equations and a linear velocity profile is predicted over the gap. We further emphasize that any stress perturbations in this parallel plate geometry are due to inertial effects alone, rendering the planar Couette setup ideal for investigating shear localization due to these effects alone.

The numerical discretization of the equations in this computational domain is performed using finite differences in one dimension (over the dashed light blue line in Fig. 1, the direction of which corresponds to the y axis) since the flow behavior is assumed homogeneous in the direction parallel to the plates. This is a feasible assumption given that the flow is laminar and the source of the inertial effects is exclusively due to the sinusoidal motion of the parallel plate. Our simulation code was implemented in the Julia language [36] whereas a suitable differential equation interface and temporal integration tools were provided by the DIFFERENTIALEQUATIONS package [37].

TABLE I. The simulation parameters applied in the dimensionless model. Note: * denotes the dimensionless normalized quantity.

Parameter	Explanation	Value
$\mathcal{N}_{NP}$	Number of nodal points	201
a	Particle size	100 μm
$w = L$	Gap width	0.04 m
v_A	LAOS amplitude	0.04 m/s
f	LAOS frequency	0.1 Hz
K_c	Shear diffusion coefficient	0.95
K_η	Viscous diffusion coefficient	1.0
D	Thermal diffusion coefficient	10^{-12} m^2/s
ϕ_0	Initial volume fraction	0.55
$\phi_{\max}$	Maximum volume fraction	0.68
ϕ_0^*	Initial (dimensionless) volume fraction	0.808
ρ	Fluid density	1000 kg/m^3
η_0	Fluid viscosity	0.001 Pas

Unless otherwise specified in the following, the parameters listed in Table I were utilized in performing the simulations. A typical simulation run time ranged from a few hours up to 2 days wall time using a single thread on an Intel® Xeon® E3-1230 CPU running at 3.40 GHz.

III. RESULTS

We will now proceed to examine the spatial particle volume fraction distributions over the gap. Furthermore, the subsequent figures will provide a qualitative examination of these volume fraction profiles as a function of the particle size a, the applied LAOS frequency f and the simulation time t. After having examined these parameters, we finally present the impact of the shear localization on the viscosity curves obtained in the simulation setup.

Figure 2 demonstrates the typical spatial volume fraction profiles over the gap as the initial dimensionless solid content ϕ_0^* is varied in a LAOS measurement. Obviously, $\phi^* = 0$ means the complete absence of the particle phase whereas $\phi^* = 1$ corresponds to the jamming limit. The

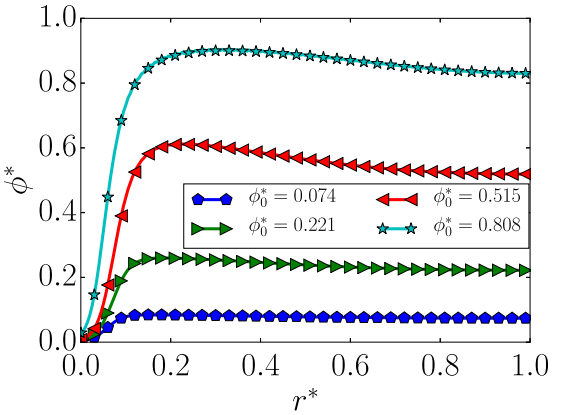

FIG. 2. The dimensionless fluid volume fraction ϕ^* versus the dimensionless gap r^*. Several initial volume fractions ϕ_0^* are displayed for the particle size $a = 100$ μm at the oscillatory frequency $f = 1.0$ Hz. Increasing ϕ_0^* produces a higher degree of concentration gradients, which, in turn, implies a higher degree of viscosity disparity between the moving ($r^* = 0$) and the stationary ($r^* = 1.0$) planes of the planar Couette setup.

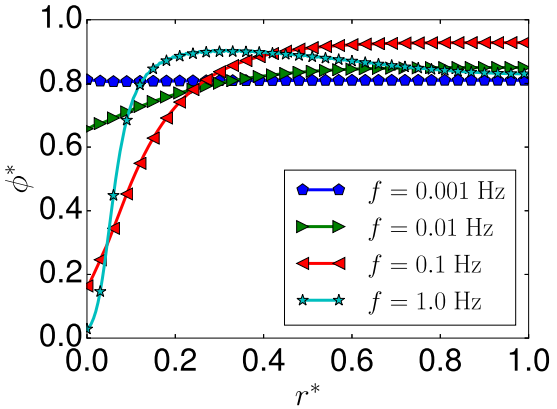

FIG. 3. The dimensionless fluid volume fraction ϕ^* versus the dimensionless gap r^*. Several frequencies f of the oscillatory shear are simulated and plotted for the particle size $a = 100$ μm. As the oscillatory frequency f at the shearing plate of the planar Couette geometry increases, the unsteady inertial terms increase as well, resulting in a strongly localized shear in the gap.

profile is obtained by running the simulation to continuous state in the cases presented here obtained after $O(10^6)$ completed sinusoidal periods. The domain close to the inner plate essentially develops into a region devoid of the solid phase, and a particle volume fraction gradient is clearly perceived over a wide range of particle volume fractions ranging from very dilute (blue curve) to semiconcentrated (cyan curve). The higher the initial volume fraction ϕ_0^*, the greater the particle volume fraction gradient and the subsequent viscosity disparity between the moving ($r^* = 0.0$) and the stationary ($r^* = 1.0$) plates [as dictated by Eq. (11)].

Figure 3 illustrates the local dimensionless solid volume fraction ϕ^* in continuous state conditions across the dimensionless measurement gap r^* for various oscillatory frequencies f. As witnessed here, higher f implies more rapid changes in the velocity at the shearing plate, corresponding to an increased level of acceleration at this plate. This inertia can be perceived as an increasing perturbation in the nonlinear equations describing the fluid structure, ultimately resulting in a more substantial localization of shear. For instance, with a relatively modest f of 1.0 Hz (cyan curve), the vicinity of the shearing plate has a very low solids content, whereas the opposite happens close to the static plate. This is due to the fact that the rapid velocity oscillations and the complementary oscillations in the shear rate (at the shearing plate) force a shear-driven diffusive flux of particles towards the static plate until these regions become jammed. Importantly, this figure illustrates that a local measurement performed at the shearing plate can hardly be regarded as the intrinsic LAOS response of a sheared homogeneous fluid with a nonlinear structural response as the one presented in this paper.

Additionally, Fig. 4 displays ϕ^* across the gap r^* for various particle sizes a. The results in this figure indicate that a suspension with large constituent size is more susceptible to higher shear localization, which seems feasible, considering that larger higher mass particles are more readily influenced by mechanical interactions in this model. Larger particles are also less sensitive to Brownian motion and the associated thermal diffusion, which would even out concentration imbalances. Interestingly, the cases corresponding to $a = 100$ and $a = 250$ μm show identical ϕ^* profiles, which suggests that the strength of the shear localization across the gap is dictated more by the frequency f of the oscillatory shear rather than the particle size a at the high particle size limit.

Having examined the spatial concentration profiles over several variables, we next quantify the degree of shear localization and then examine this as a function of the model parameters. To this end, the interface serving as the boundary between areas of distinct viscosities would clearly merit attention. However, the previous figures clearly indicate that the localization for this type of structural

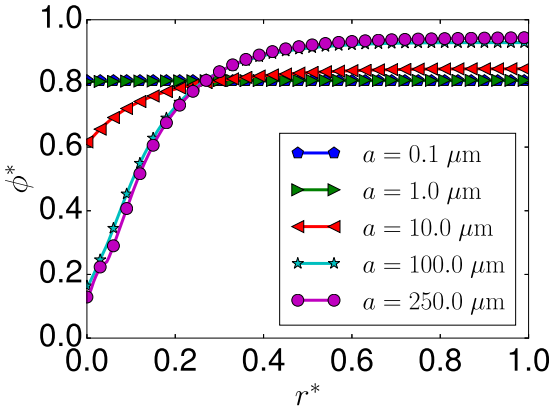

FIG. 4. The dimensionless fluid volume fraction ϕ^* versus the dimensionless gap r^* plotted for several particle sizes a whereas the oscillatory frequency f remains constant (0.1 Hz). Larger particles are more susceptible to mechanical interactions and less influenced by thermal diffusion, implying a stronger tendency to shear localization due to diffusive fluxes.

response is continuous in nature, owing to the conservation of particles (mass) across the gap and the diffusive nature of the problem. Therefore, we propose to quantify the degree of flow localization by examining the variance in the local Reynolds number, expressed as $\mathrm{Re} = \rho UL/\eta$. Now, we define $C_v = \sigma_{\mathrm{Re}}/\langle \mathrm{Re} \rangle$ with $\sigma^2_{\mathrm{Re}} = \int_0^1 (\mathrm{Re} - \langle \mathrm{Re} \rangle)^2 dr^*$ and $\langle \mathrm{Re} \rangle = \int_0^1 \mathrm{Re}\, dr^*$, which describes the spatial variance of the local Reynolds number in the system, normalized over the averaged Reynolds number. This quantity, thus, bears close resemblance to the concept of the coefficient of variation and can be employed to study the departures from the idealized homogeneous viscosity profile across the gap. Figure 5 depicts a contour plot, where C_v contours are spanned over a wide range of the LAOS oscillation frequency f and the particle size a. As expected based on the previous results, the strength of shear localization increases as either f or a is increased. At low f, the inertial

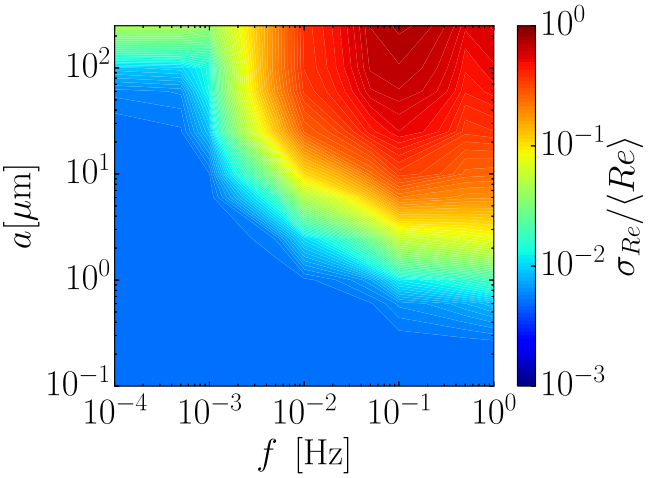

FIG. 5. The coefficient of variation of the Reynolds number $\sigma_{\mathrm{Re}}/\langle \mathrm{Re} \rangle$, which quantifies the strength of the shear localization in each case, is given in this contour plot as a function of the oscillatory frequency f and the particle size a. High f and a, subsequently, produce higher shear localization, as expected. However, the degree of localization has a maximum at around $f = 0.1$ Hz for the largest particle sizes. This rather puzzling result is discussed more in conjunction with Fig. 8.

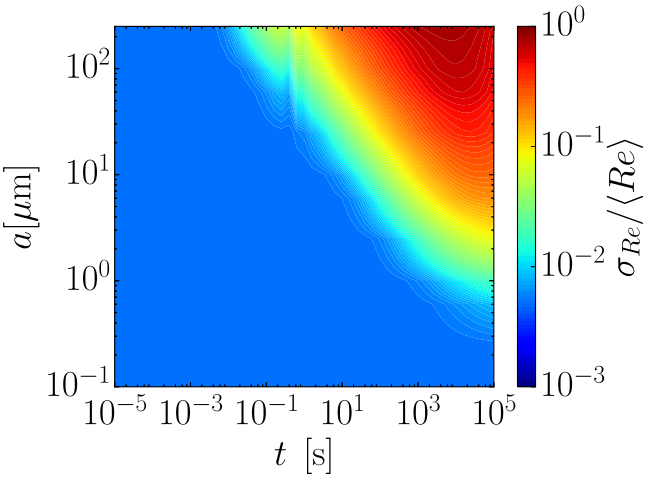

FIG. 6. The coefficient of variation of the dimensionless viscosity $\sigma_{\mathrm{Re}}/\langle\mathrm{Re}\rangle$ is depicted in this contour plot as a function of the simulation time t and the particle size a whereas the oscillation frequency is fixed at $f = 0.1$ Hz. With time, the degree of localization C_v becomes more pronounced. From a theoretical point of view, this is expected since the oscillatory perturbation keeps forcing the nonlinear structural response in the diffusion equation and the subsequent shear localization effect.

perturbation is weak and does not induce significant shear localization (low values of C_v). However, with increased f, C_v increases exponentially, finally reaching a maximum value signifying the maximum degree of shear localization attainable for the given particle size a in question. For large particle sizes a, however, C_v also decreases after having passed this maximum as f is increased even further, which will be addressed later in the commentary regarding Fig. 8. On a general level, larger particles (large a) are more affected by the shear-driven mechanisms and experience a more pronounced heterogeneous concentration profile in the continuous state. Increasing the relative strength of the inertial perturbation at the oscillating plate (increasing f) also provides a higher C_v, translating to a higher degree of shear localization. Thus, it seems shear localization may occur as a mundane part of LAOS for particulate suspensions and is negligible only for extremely small constituent sizes (high diffusion and Péclet number due to ambient temperature) and oscillatory frequencies.

The previous results map out the degree of shear localization in the continuous state for a and f. However, the temporal evolution of C_v is also of fundamental importance since this defines whether significant localization is witnessed on timescales comparable to those employed in typical LAOS experiments. This issue is addressed in Fig. 6 where a contour plot similar to that in Fig. 5 is displayed. Now, on the x axis, t describes the total simulation time [in *Système International* (SI) units]. As one would logically expect, the degree of shear localization amplifies monotonically as the LAOS progresses in time: The sinusoidal oscillatory shear instilled at the shearing plate is delivered repeatedly to the system, and the resulting nonlinear response is amplified more as this perturbation is introduced over and over again (increasing t). This progression is examined in more depth in Fig. 7 where several curves corresponding to specific lines with constant a in Fig. 6 are plotted. Qualitatively, $\sigma_{\mathrm{Re}}/\langle\mathrm{Re}\rangle$ increases exponentially as a function of the simulation time t. Specifically for larger particles, representative of, e.g., granular particles in the experimental realm, C_v obtains significant values already as t reaches $O(1)$ s, which is certainly on a par with the experimental timescales. This is in stark contrast to the original study of the model in a cylinder Couette device by Phillips *et al.* [29] where time scales well in excess of a typical duration of an experiment were required for significant concentration heterogeneities to develop. Consequently, this suggests that strong shear localization be addressed as an integral part in a LAOS measurement of a complex fluid with shear-driven diffusive interactions. We further note that due to the very general nature of

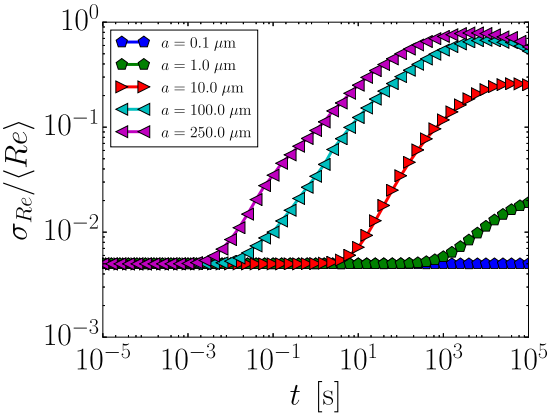

FIG. 7. The coefficient of variation C_v versus the simulation time t plotted for several particles sizes a (with fixed $f = 0.1$ Hz). Especially for larger particles, the degree of localization increases exponentially, beginning well below the typical timescale of observation $O(1)$.

these mechanical interactions, they are arguably present in many complex fluids under shear and are not exclusively restricted to suspensions of repulsive hard spheres.

Finally, Fig. 8 represents inverse of the averaged viscous timescale [see Eq. (18)] over a wide frequency range of the oscillatory shear for several particle sizes. In essence, $\langle\tau_{\text{visc}}\rangle$ describes the typical timescale in which the fluid is capable of viscously dissipating the imposed shear over the gap. This, in turn, is plotted here as a function of the inverse timescale of the oscillation ($f = 1/\tau_{LAOS}$). The onset of shear localization is perceived as a sudden increase in $\langle\tau_{\text{visc}}\rangle$, which seems plausible: Regions of higher and lower concentrations developing due to this localization translate to similar regions of distinct viscosities according to our model. Due to the nonlinear nature of Eq. (11), regions of higher concentration contribute more to this average and accordingly as shear localization progresses, $\langle\tau_{\text{visc}}\rangle$ increases. Interestingly, the onset of the localization seems to occur at $\tau_{\text{visc}} \approx \tau_{LAOS}$ regardless of the suspension particle size a, or the applied LAOS amplitude v_a based on our simulations since the two latter variables only contribute to the strength of the shear

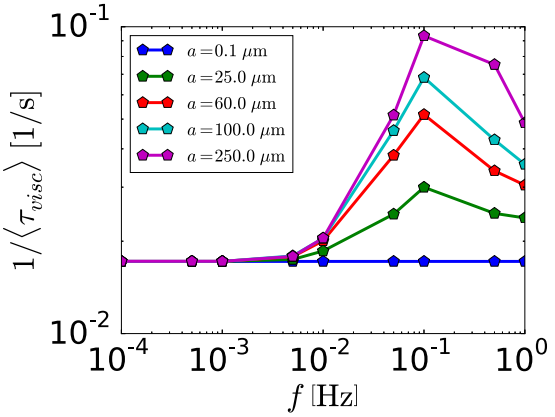

FIG. 8. The inverse of the averaged viscous timescale $\langle 1/\tau_{\text{visc}}\rangle$ versus the oscillatory frequency f for several particle sizes a. Here, $\langle 1/\tau_{\text{visc}}\rangle$ represents the inverse timescale of the Navier-Stokes equation, whereas f represents the inverse timescale of the oscillation. Judging by this figure, the localization begins to increase markedly only when these timescales coincide.

localization response and not to its onset criterion. That is, perturbations with longer timescales than the typical fluidization time, dependent on the given gap and initial particle volume fraction, do not efficiently induce shear localization. Once the two coincide, shear localization commences with suspensions containing larger particle sizes being susceptible to higher degrees of localized shear. Therefore, $\langle \tau_{\mathrm{visc}} \rangle$ increases up until the gap region in close proximity of the shearing plate has become sufficiently devoid of the suspended medium. At this point, the fluidization time in this region is significantly longer than the timescale of the oscillatory shear, and the oscillatory shear is, therefore, no longer transmitted sufficiently fast across the gap to induce more localization. Thus, the degree of shear localization has reached its peak at this point. For experimentalists working with suspensions prone to shear-driven diffusion seeking a reasonable rule of thumb, the inverse viscous timescale ($\eta/\rho L^2$) evaluated based on the initial suspension viscosity, density, and measurement gap presents the limit for the LAOS frequency, beyond which significant shear localization could be reasonably expected.

IV. CONCLUSIONS

In this paper, a simple model system for a complex fluid, a hard-sphere suspension with two-body collisions and subsequent shear-driven diffusion, is examined in (LAOS) in a planar Couette device. We perform simulations employing this model, which predicts monotonic intrinsic flow curves for the system. Significantly, we observe a decrease in particle volume fraction close to the moving wall. Due to the available viscosity contrast, this is manifested as wall slip at small particle volume fractions and a high degree of shear localization at high particle volume fractions. Importantly, these form in the relatively simple planar Couette geometry employed here, although simple shear flow would routinely be expected. The rationale behind this shear localization is the accelerating motion of the plate imposing the oscillatory shear, which serves as a perturbation in the nonlinear equations describing the structural response of the complex fluid to shear, resulting in nonhomogeneous spatial concentration profiles across the measurement gap.

Although the model was nondimensionalized to provide better numerical stability in simulations, the constituent size (a) and LAOS frequency f are presented primarily in SI units to render the results more accessible to the reader. By defining the coefficient of variance of the Reynolds number $C_v = \sigma_{\mathrm{Re}}/\langle \mathrm{Re} \rangle$, the strength of the shear localization could be conveniently quantified and was shown to exhibit exponential growth as a function of both the oscillatory frequency f and the total duration of the simulation t whereas increasing a and f implied both a higher degree of shear localization and a faster temporal evolution of the system towards the heterogeneous state. We also stress that the relatively simple shear-driven diffusive mechanisms considered here that are sufficient to trigger the localized shear response should be ubiquitous among the various classes of complex fluids with an embedded discrete phase. The results, therefore, indicate that shear localization is an inherent part of a typical LAOS scenario, and ignoring its role may lead to erroneous conclusions regarding the properties of a complex fluid.

Therefore, we are intrigued by the possibility of further experimental work utilizing, for instance, magnetic resonance imaging, optical coherence tomography, and various microscopy techniques conducted by experimentalists on various samples under the LAOS protocol. Based on our previous experiences, a standard rheological measurement of a sample utilizing a rheometer enhanced with tomographic imaging capabilities could prove to be a suitable candidate for experimentally probing the localization response. Specifically, accessing the local spatial density (concentration) profile during the experiment could, in our view, provide a valuable new insight on the prevalence of shear localization due to concentration gradients in a wide array of complex fluids.

ACKNOWLEDGMENTS

We wish to thank the Jane and Aatos Erkko Foundation for their financial support via the NANOFORM Project and the Aalto Science-IT Project for the high-performance computational

resources. The financial support of the Academy of Finland (Project No. 278367) is also greatly appreciated.

[1] H. Barnes, A review of the slip (wall depletion) of polymer solutions, emulsions and particle suspensions in viscometers: its cause, character, and cure, J. Non-Newton. Fluid. **56**, 221 (1995).
[2] M. Cloitre and R. Bonnecaze, A review on wall slip in high solid dispersions, Rheol. Acta **56**, 283 (2017).
[3] G. Ovarlez, S. Rodts, X. Chateau, and P. Coussot, Phenomenology and physical origin of shear localization and shear banding in complex fluids, Rheol. Acta **48**, 831 (2009).
[4] M. Mohtaschemi, A. Puisto, X. Illa, and M. Alava, Rheology dynamics of aggregating colloidal suspensions, Soft Matter **10**, 2971 (2014).
[5] T. Divoux, M. Fardin, S. Manneville, and S. Lerouge, Shear banding of complex fluids, Annu. Rev. Fluid Mech. **48**, 81 (2016).
[6] R. Benzi, T. Divoux, C. Barentin, S. Manneville, M. Sbragaglia, and F. Toschi, Unified Theoretical and Experimental View on Transient Shear Banding, Phys. Rev. Lett. **123**, 248001 (2019).
[7] K. Hyun, M. Wilhelm, C. Klein, K. S. Cho, J. G. Nam, K. H. Ahn, S. J. Lee, R. Ewoldt, and G. McKinley, A review of nonlinear oscillatory shear tests: Analysis and application of large amplitude oscillatory shear (LAOS), Prog. Polym. Sci. **36**, 1697 (2011).
[8] S. M. Fielding and P. D. Olmsted, Spatiotemporal Oscillations and Rheochaos in a Simple Model of Shear Banding, Phys. Rev. Lett. **92**, 084502 (2004).
[9] P. Olmsted, Perspectives on shear banding in complex fluids, Rheol. Acta **47**, 283 (2008).
[10] T. Divoux, D. Tamarii, C. Barentin, and S. Manneville, Transient Shear Banding in a Simple Yield Stress Fluid, Phys. Rev. Lett. **104**, 208301 (2010).
[11] S. Fielding, Triggers and signatures of shear banding in steady and time-dependent flows, J. Rheol. **60**, 821 (2016).
[12] K. G. and N. Wagner, Large amplitude oscillatory shear (LAOS) measurements to obtain constitutive equation model parameters: Giesekus model of banding and nonbanding wormlike micelles, J. Rheol. **56**, 333 (2012).
[13] M. Armstrong, A. Beris, S. Rogers, and N. Wagner, Dynamic shear rheology of a thixotropic suspension: Comparison of an improved structure-based model with large amplitude oscillatory shear experiments, J. Rheol. **60**, 433 (2016).
[14] M. Fardin, C. Perge, L. Casanellas, T. Hollis, N. Taberlet, J. Ortín, S. Lerouge, and S. Manneville, Flow instabilities in large amplitude oscillatory shear: a cautionary tale, Rheol. Acta **53**, 885 (2014).
[15] R. Radhakrishnan and S. M. Fielding, Shear Banding of Soft Glassy Materials in Large Amplitude Oscillatory Shear, Phys. Rev. Lett. **117**, 188001 (2016).
[16] L. Zhou, P. Cook, and G. McKinley, Multiple shear-banding transitions for a model of wormlike micellar solutions, SIAM J. Appl. Math. **72**, 1192 (2012).
[17] K. A. Carter, J. M. Girkin, and S. M. Fielding, Shear banding in large amplitude oscillatory shear (LAOStrain and LAOStress) of polymers and wormlike micelles, J. Rheol. **60**, 883 (2016).
[18] D. Leighton and A. Acrivos, The shear-induced migration of particles in concentrated suspensions, J. Fluid Mech. **181**, 415 (1987).
[19] V. Breedveld, D. van den Ende, M. Bosscher, R. J. J. Jongschaap, and J. Mellema, Measuring shear-induced self-diffusion in a counterrotating geometry, Phys. Rev. E **63**, 021403 (2001).
[20] D. Semwogerere and E. Weeks, Shear-induced particle migration in binary colloidal suspensions, Phys. Fluids **20**, 043306 (2008).
[21] A. Fall, F. Bertrand, G. Ovarlez, and D. Bonn, Shear thickening of cornstarch suspensions, J. Rheol. **56**, 575 (2012).
[22] R. G. Henríquez Rivera, X. Zhang, and M. D. Graham, Mechanistic theory of margination and flow-induced segregation in confined multicomponent suspensions: Simple shear and Poiseuille flows, Phys. Rev. Fluids **1**, 060501 (2016).

[23] M. Korhonen, M. Mohtaschemi, A. Puisto, X. Illa, and M. J. Alava, Start-up inertia as an origin for heterogeneous flow, Phys. Rev. E **95**, 022608 (2017).
[24] A. Jain, R. Singh, L. Kushwaha, V. Shankar, and Y. Joshi, Role of inertia and thixotropy in start-up flows of aging soft materials: Transient dynamics and shear banding in a rate-controlled flow field, J. Rheol. **62**, 1001 (2018).
[25] S. Fielding and P. Olmsted, Flow phase diagrams for concentration-coupled shear banding, Eur. Phys. J. E **11**, 65 (2003).
[26] R. Besseling, L. Isa, P. Ballesta, G. Petekidis, M. E. Cates, and W. C. K. Poon, Shear Banding and Flow-Concentration Coupling in Colloidal Glasses, Phys. Rev. Lett. **105**, 268301 (2010).
[27] M. Cromer, M. Villet, G. Fredrickson, and L. Leal, Shear banding in polymer solutions, Phys. Fluids **25**, 051703 (2013).
[28] V. Breedveld, D. van den Ende, R. Jongschaap, and J. Mellema, Shear-induced diffusion and rheology of noncolloidal suspensions: Time scales and particle displacements, J. Chem. Phys. **114**, 5923 (2001).
[29] R. Phillips, R. Armstrong, R. Brown, A. Graham, and J. Abbott, A constitutive equation for concentrated suspensions that accounts for shear-induced particle migration, Phys. Fluids A **4**, 30 (1992).
[30] V. Baranau and U. Tallarek, Random-close packing limits for monodisperse and polydisperse hard spheres, Soft Matter **10**, 3826 (2014).
[31] H. Shewan and J. Stokes, Analytically predicting the viscosity of hard sphere suspensions from the particle size distribution, J. Non-Newton. Fluid. **222**, 72 (2015).
[32] J. Stickel and R. Powell, Fluid mechanics and rheology of dense suspensions, Annu. Rev. Fluid Mech. **37**, 129 (2005).
[33] E. Brown and H. Jaeger, The role of dilation and confining stresses in shear thickening of dense suspensions, J. Rheol. **56**, 875 (2012).
[34] M. Hermes, B. Guy, W. Poon, G. Poy, M. Cates, and M. Wyart, Unsteady flow and particle migration in dense, non-Brownian suspensions, J. Rheol. **60**, 905 (2016).
[35] E. Brown and H. Jaeger, Shear thickening in concentrated suspensions: phenomenology, mechanisms and relations to jamming, Rep. Prog. Phys. **77**, 046602 (2014).
[36] J. Bezanson, A. Edelman, S. Karpinski, and V. Shah, Julia: A fresh approach to numerical computing, SIAM Rev. **59**, 65 (2017).
[37] C. Rackauckas and Q. Nie, DifferentialEquations.jl-A performant and feature-rich ecosystem for solving differential equations in Julia, J. Open Res. Software **5**, 15 (2017).